Measurement of aberrations in microlenses using a Shack-Hartmann wavefront sensor

Paul D. Pulaski, James P. Roller, Daniel R. Neal, Keith Ratte
Wavefront Sciences, Inc.

ABSTRACT

We have measured the wavefront aberrations of fused silica and silicon microlenses using a Shack-Hartmann wavefront sensor system. The Shack-Hartmann sensor uses a combination of a microlens array and a CCD camera to measure wavefront local tilts with respect to a reference wavefront. Data reduction software then reconstructs the wavefront and expresses it in various forms such as Seidel or Zernike. We measured a series of our custom microlens arrays by placing a fiber source at a distance of one focal length behind the array to create a series of collimated beams from the individual lenslets. We then observed the quality of the collimated beams from single lenslets by using different aperture converters (for different sized lenslets) to expand the individual beams so that they filled a significant portion of the CCD area. For these microlens arrays, the P-V OPD was found to be less than λ/4 and the RMS wavefront error less than λ/20.

1. INTRODUCTION

In recent years, there has been a growing demand for various types of microlenses. Applications range from light coupling in optical communication systems to lenslet arrays in wavefront sensors. With this rise in applications, there is a need for precision testing of the quality of the microlenses. The most common technique for measuring the wavefront aberrations of optical systems is the use of an interferometer, which requires vibration-isolation platforms, a reference beam and tedious alignment procedures.

An alternative to the interferometric techniques for measuring microlenses[1] is the use of a Shack-Hartmann wavefront sensor that does not require any vibration-isolation and the alignment is fairly straightforward. The Shack-Hartmann sensor uses a micro-optic lenslet that is mounted in front of a CCD array in order to measure the wavefront characteristics of a light beam that is either transmitted through an optical element or reflected off of an optical surface such as a lens or mirror. The light is sampled by the individual lenslets that create a series of focal spots under each lenslet onto the finely spaced CCD array. These focal spots positions are measured and the center of the spots (known as the centroids) are calculated by determining their center-of-mass coordinates. The centroid positions from the focal spots of the test beam are compared with the centroid positions from a carefully constructed reference file. This reference file allows for the minimization of effects from imperfections in the CCD array, lenslet arrays and imaging system. From this data, the average gradient of the wavefront over each lenslet can be calculated from the difference between the centroid positions and those of the reference wavefront, which can be integrated to provide the reconstructed wavefront of the incident radiation. The wavefront $\phi(x,y)$ can be calculated from the gradient equation:

$$\nabla\phi(x,y) = \theta_x(x,y,)\hat{i} + \theta_y(x,y,)\hat{j}$$

where θ_x and θ_y are functions of the measured slope data which resolve to following differential equations:

$$\frac{\partial\phi}{\partial x} = \theta_x \quad \text{and} \quad \frac{\partial\phi}{\partial y} = \theta_y$$

These equations can be solved by using either zonal or modal methods in order to reconstruct the wavefront. The modal method reconstructs the wavefront within a circular mask that is determined by the user. The output can be a set of weighted Zernike polynomials as defined in Malacara[2] that relate to the aberrations present in the wavefront. The zonal

method follows in principle the formulation of Southwell[3], which derives a set of relations for the phase given a number of slope measurements. The phase at a given point can be predicted from the four adjacent points using this successive over relaxation technique.

1.1 Micro-optics fabrication

There are a multitude of techniques to fabricate micro-optics, which include molding technology, ink-jet printing technology, and photolithography. The micro-optic fabrication technique that we use falls into the latter category. The process includes designing a gray-scale mask that is used to photolithographically pattern a photoresist-coated substrate (either fused silica or silicon) and then fabricating of the microlenses or diffractive optical elements. The gray-scale mask has a high-resolution pattern with a range of optical densities (OD) that are used in the photolithographic process to pattern the photoresist. This pattern is then etched into the substrate using a plasma-etch process. Normally, each microlens has at least 32 levels, which are used to approximate the contour of the surface of the lens. We can manufacture any shape lenslet, however our standard lenslet arrays are made up of square lenslets with a 100 % fill factor.

2. MEASUREMENT SETUP

A diagram of the setup used to make the transmission measurements is shown in Figure 1 and the reflection measurement setup is shown in Figure 2. The main elements include a single mode fiber coupled to a 635 nm diode laser source, an aperture converter and the wavefront senor. The transmission measurements were taken by placing a fiber laser source at a focal distance behind the test lenslet array. By masking off the largest circle enclosing the wavefront from an individual lenslet, the position of the lenslet relative to the fiber point source was moved until we obtained the largest radius of curvature, which is calculated from the $c_{2,1}$ coefficient of the associated Zernike term. This insured a "collimated" output beam incident on the wavefront sensor. The reflection measurements were taken with a collimated light source incident on the silicon lenslet arrays. The reflected wavefront then passes through the aperture converter and into the wavefront sensor.

The first step to making wavefront measurements with the Shack-Hartmann sensor is to create a reference file of a collimated beam using a precision lens that has a wavefront error $<\lambda/100$ over the center 1 mm^2 area of the lens and shear plate for collimation. All the subsequent measurements were taken with respect to this reference file. The wavefront slopes at each lenslet are calculated from the difference between the measured and the referenced centroid positions.

In order to avoid confusion, we need to note that there are two types of lenslet arrays in this setup. First, there is the lenslet array that is part of the wavefront sensor and then there are the different lenslet arrays that were actually tested. The lenslet array that was mounted on the sensor camera had a focal length of 25.1 mm and a diameter of 0.252 mm for the transmission measurements. This particular lenslet array yields one of the highest sensitivities but nearly the lowest dynamic range of our sensor camera options, given the relatively long focal length. In this set of experiments, sensitivity was more important than dynamic range, given the small aberrations of these individual lenslets that we tested. The tradeoff was that the sensor lenslets had a lower spatial resolution, and thus fewer data points than the other available lenslets. In the future we plan to fabricate longer focal length lenses with higher spatial resolution (smaller diameters) for our sensors to test various types of micro-optics including lenslet arrays, microlenses and small aspheres. The lenslet array that was mounted on the sensor camera for the reflection measurements had lenslets with a focal length of 8.1 mm and a diameter of 0.144 mm. In this case, a higher spatial resolution was needed to faithfully reproduce the surface of the silicon lenslets used in the reflection mode.

Depending on the size of the individual lenslets, the aperture converters were designed to expand the beam so that the image from a single lenslet filled a significant portion of the CCD sensor area. Three fused silica lenslet arrays were measured in transmission and two silicon lenslet arrays were measured in reflection using the fiber-coupled diode laser source. Details of the lenslet parameters and the type of aperture converter used to magnify the image of the individual lenslets are shown in Table 1. Both circular and square software masks were used to select a portion of the total image pattern for post processing the wavefront slope data. The circular masks allow us to analyze the data as a reconstruction into Zernike polynomials. In this case the mask enclosed the largest circular pattern within an individual lenslet. By

masking off the whole enclosed pattern of a square lenslet, zonal methods were used to reconstruct the wavefront. The latter yields critical information regarding the wavefront from the total area of a single lenslet.

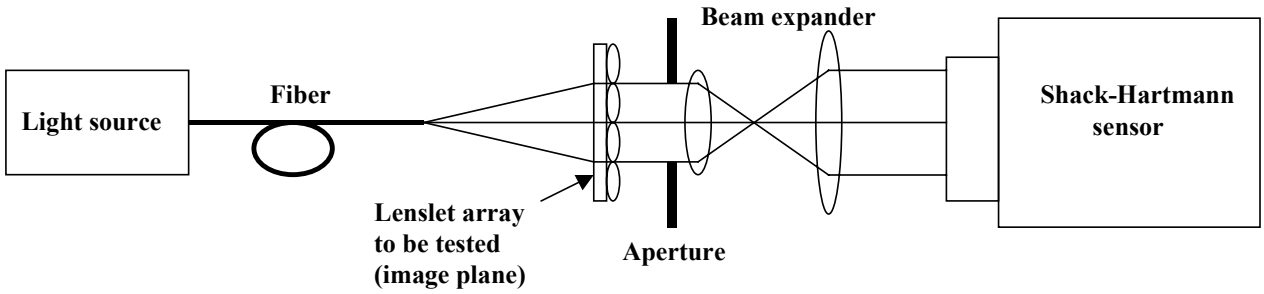

Figure 1: Setup to measure the wavefront aberrations of fused silica microlenses in transmission mode.

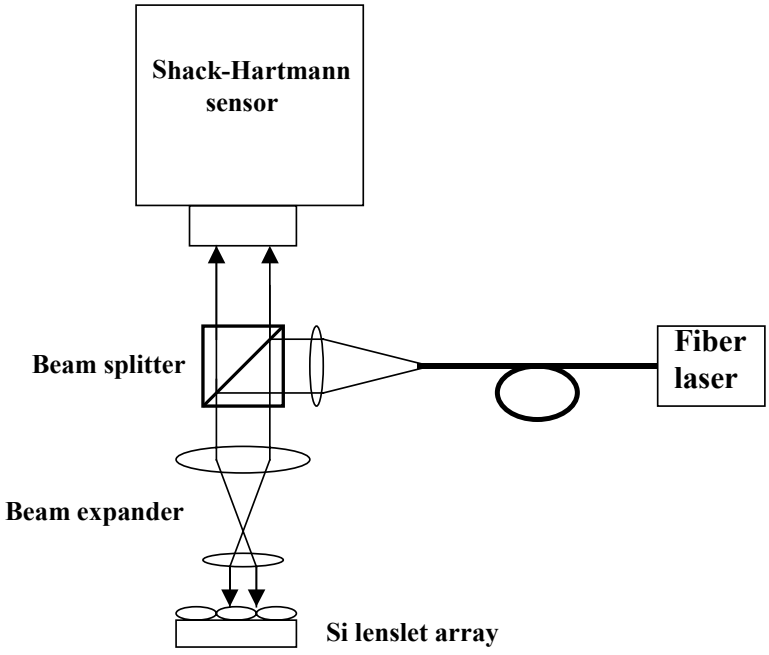

Figure 2: Setup to measure the wavefront aberrations of silicon microlenses in reflection mode.

Lenslet array	Focal length (mm)	Diameter (mm)	Aperture Converter
Fused silica	**8.2**	**0.144**	**22 X**
Fused silica	**15.5**	**0.198**	**22 X**
Fused silica	**25.1**	**0.252**	**16 X**
Silicon	**16.8**	**0.320**	**7.9X**
Silicon	**25.7**	**0.400**	**7.9X**

Table 1: Test lenslet array specifications.

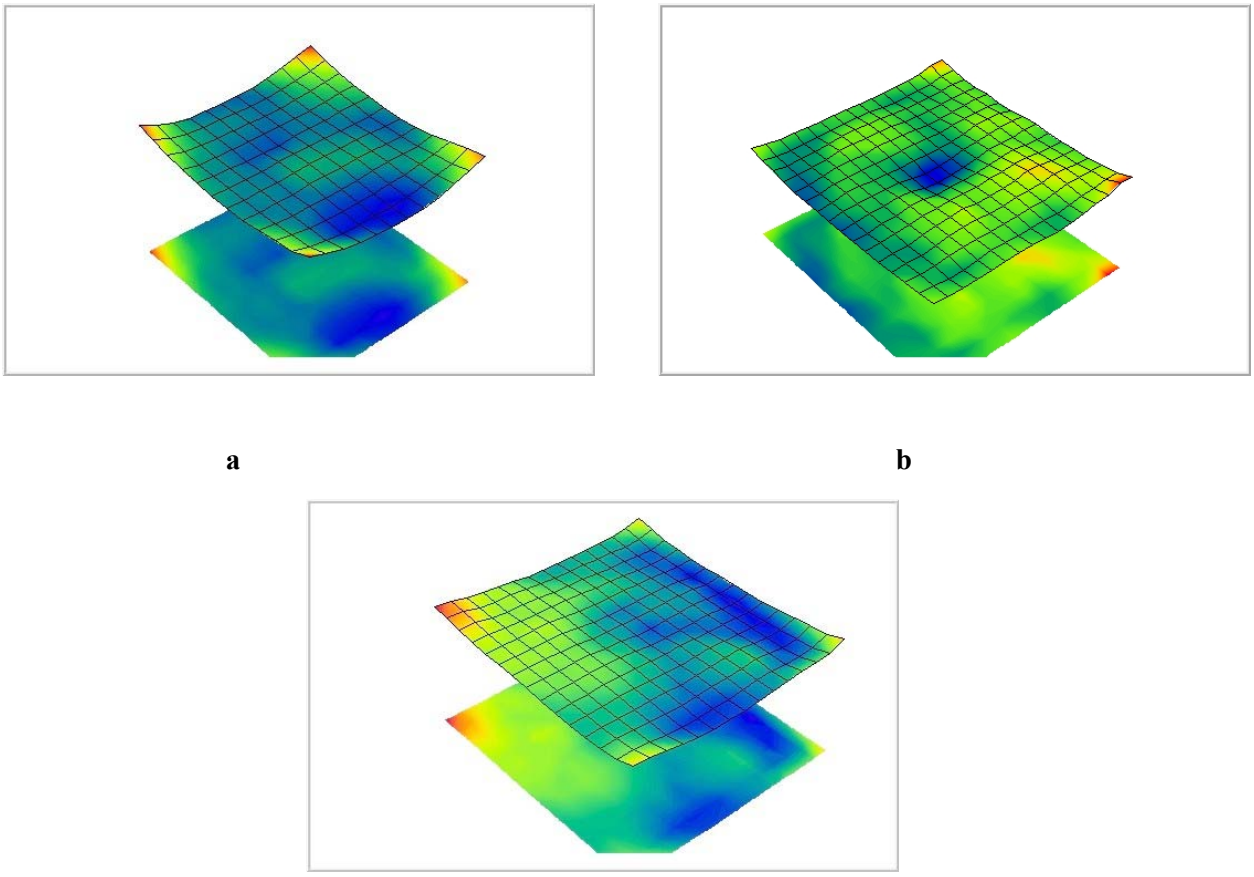

a **b**

c

Figure 3: Zonal wavefront phase map of individual fused silica lenslets with:
a) Focal length = 8.2 mm ; diameter = 0.144 mm, P-V OPD = 0.1246 μm
b) Focal length = 15.5 mm ; diameter = 0.198 mm, P-V OPD = 0.0798 μm
c) Focal length = 25.1mm ; diameter = 0.252 mm, P-V OPD = 0.1059 μm

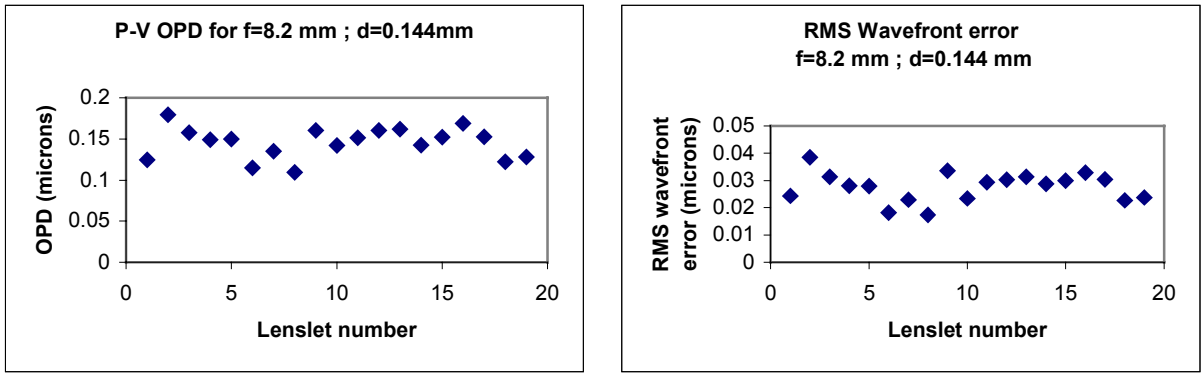

Figure 4: Zonal wavefront OPD and RMS Wavefront error for fused silica lenslets with focal length= 8.2 mm ; diameter= 0.144 mm

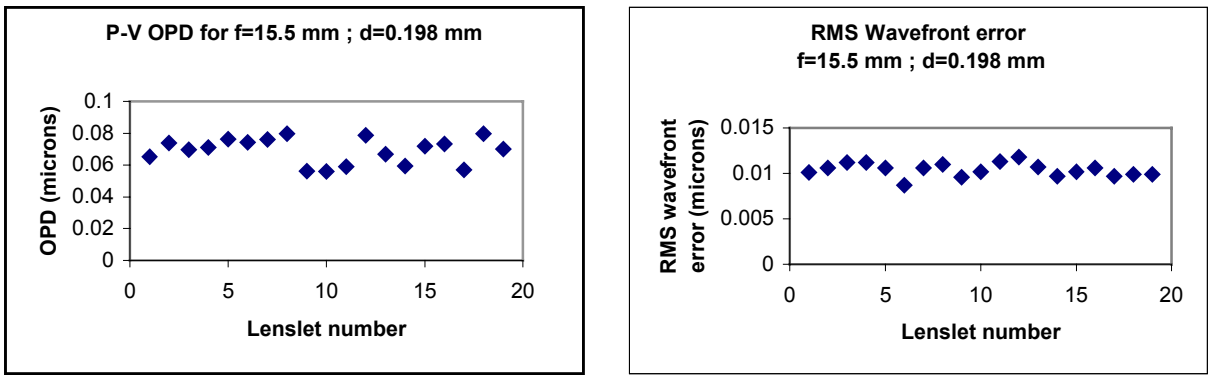

Figure 5: Zonal wavefront OPD and RMS Wavefront error for fused silica lenslets with focal length= 15.5 mm ; diameter= 0.198 mm

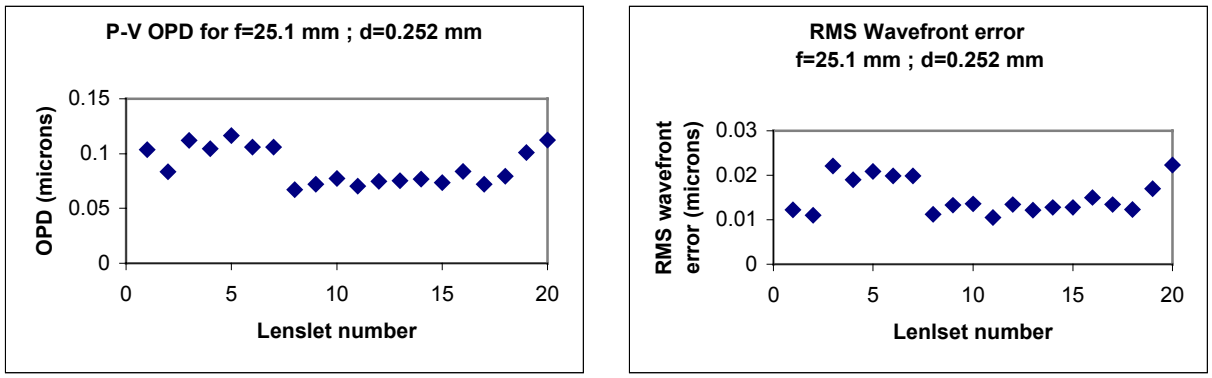

Figure 6: Zonal wavefront OPD and RMS Wavefront error for fused silica lenslets with focal length= 25.1 mm ; diameter= 0.252 mm

Lenslet type	Average P-V OPD in waves	Average OPD RMS in waves
f= 8mm ; d=0.144mm	0.229	0.044
f= 15mm ; d=0.198mm	0.109	0.016
f= 25mm ; d=0.252mm	0.137	0.023

Table 2: Average P-V OPD and RMS wavefront error in waves for the fused silica lenslets

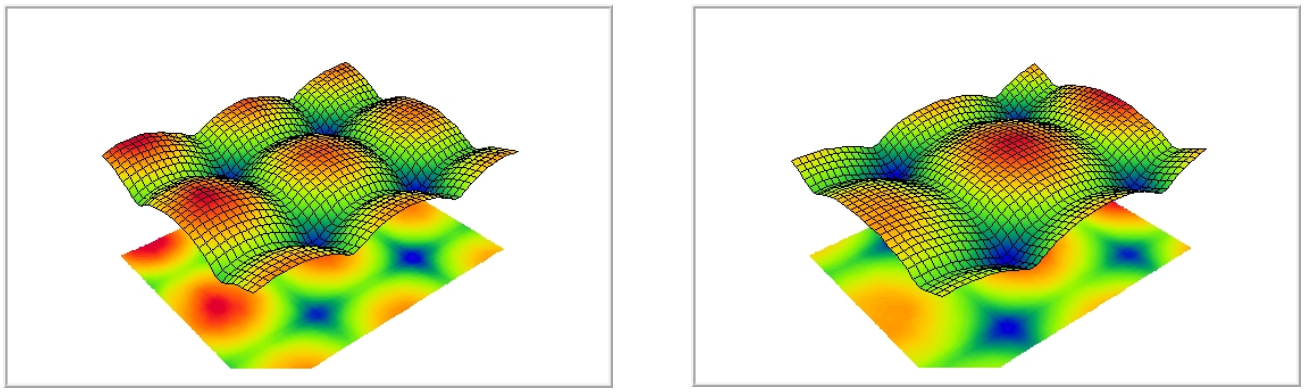

a **b**

Figure 7: Zonal wavefront phase map for silicon lenslets; a) f=16.5mm, d=0.320mm, b) f=25.7mm, d=0.400mm

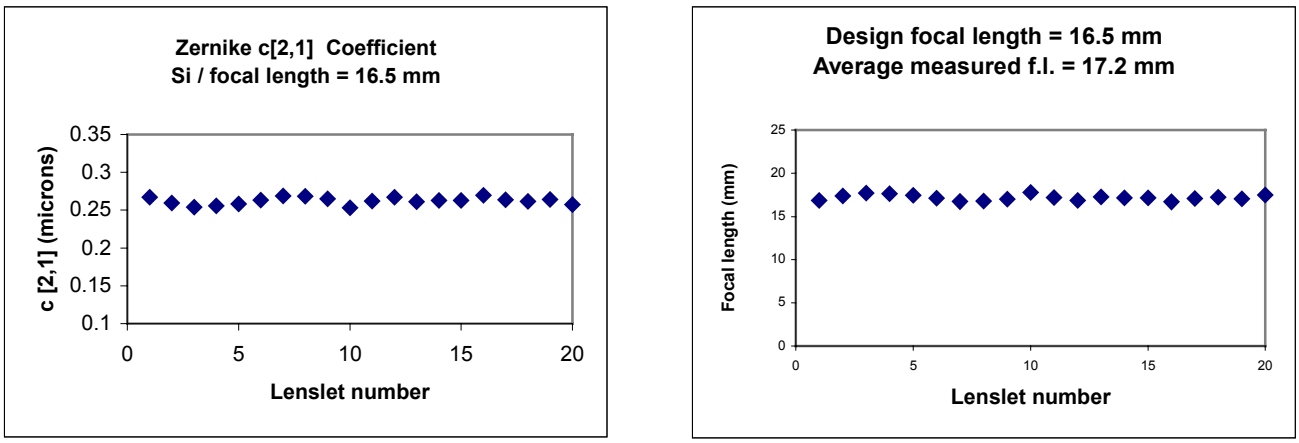

Figure 8: Zernike $c_{2,1}$ coefficient and focal length for silicon lenslets; a) f = 16.5mm, d = 0.320mm

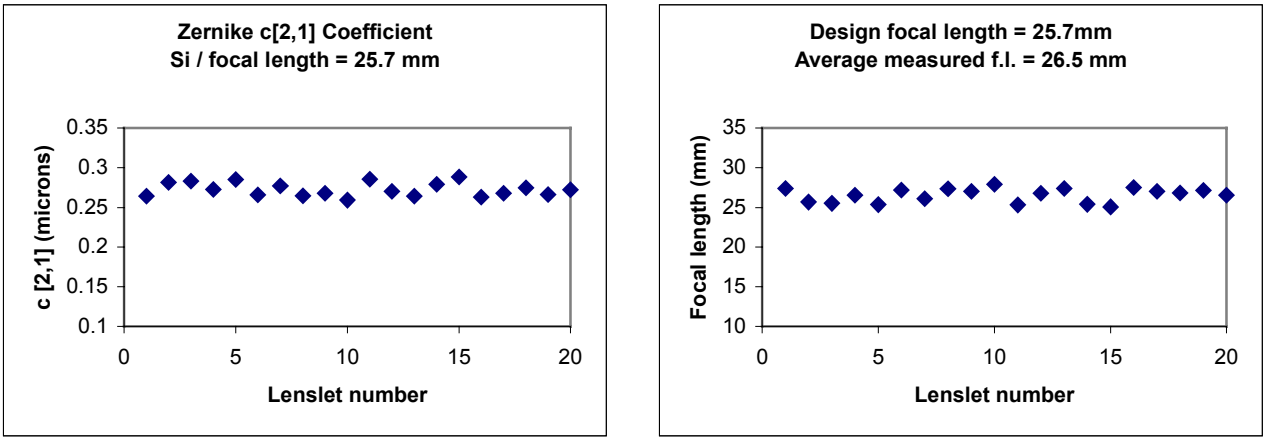

Figure 9: Zernike $c_{2,1}$ coefficient and focal length for silicon lenslets; a) f = 25.7mm, d = 0.400mm

3. WAVEFRONT MEASUREMENTS

Using the setup in Figure 1, the transmitted wavefront of the fused silica lenslets was measured. We took a random sampling of 20 individual lenslets from each of the three test fused silica arrays. For each position of an individual lenslet, the wavefront measurement was averaged over 100 frames to reduce the effects of air turbulence. Both circular and square masks were used to reconstruct the wavefront via the modal and zonal methods respectively. By analyzing the Zernike decomposition of the waverfront from these lenslets with our modal method, we found that apart from the tilt terms, there was a negligible contribution from higher order terms, which indicates that the Seidel aberrations such as astigmatism, coma and spherical aberration do not play a significant role in the transmitted wavefront through these lenslets. At first there appeared to be a contribution to the total wavefront from the $c_{4,2}$ term (which relates to the 3rd order spherical aberration), however upon closer inspection, it was revealed that this coefficient was not sufficiently large to indicate that spherical aberration was actually present in the wavefront. Therefore, the zonal method was used to reconstruct the wavefront with a square mask enclosing the total area of an individual lenslet. The relevant parameters that were measured in this case are the P-V optical path difference (OPD) and the RMS wavefront variation (or wavefront error). The OPD is the total peak-to-valley phase difference across the enclosed mask area and the RMS variation is the root-mean-square of the reconstructed wavefront from the average OPD. Representative 3-D plots of the reconstructed wavefronts from each of the three fused silica lenslet arrays are shown in Figure 3. In addition, the OPD and the associated RMS wavefront variations of all the measured fused silica lenslets are plotted in Figures 4, 5, and 6. In addition, the average P-V OPD and RMS wavefront error for these test lenslet arrays is shown in Table 2.

From this data, one can see that the smallest diameter lenslet yields a significantly larger OPD and wavefront error. This could be due to the fact that the f = 8.2 mm lenslet array has the smallest lateral feature sizes in the levels used to approximate the contour of the lenslets, compared to the other two test arrays. As this feature size decreases, there could be a slight degradation in the surface quality due to limitations in the fabrication process (especially near the corners of the lenslets), leading to more aberration of the transmitted wavefront. There is a slightly enhanced deformation of the zonal OPD near the corners of all three test lenslets, however this effect is more pronounced for the smallest lenslet.

Reflection wavefront measurements of the silicon lenslets were also performed on a series of 20 random lenslets from two of our standard silicon lenslet arrays. For this case, a collimated beam was incident on the surface of the lenslet arrays, with the reflected wavefront measured by the sensor as shown in Figure 2. For these measurements, we used the

zonal method to construct the phase map of the surface (Figure 7), and the modal method to reconstruct the wavefront into a series of Zernike polynomials. Again the higher order Zernike terms relating to the Seidel aberrations were negligible except for the Zernike coefficient ($c_{2,1}$) that is used to calculate the radius of curvature. This term obviously played a significant contribution given that the design shape of the contour of the individual lenslets is practically spherical. The radius of curvature for these reflection measurements can be calculated as follows:

$$R_c = \frac{R_z^2}{4(\frac{1}{2}c_{2,1})}$$

where R_z is a scale factor that relates to the size of the circular Zernike mask. From this value for the radius of curvature, the focal length of the individual lenses can be calculated through the expression:

$$f = \frac{R_c}{n-1}$$

where f is the focal length and n is the index of refraction of the lenslet material. The focal lengths were calculated for silicon at a wavelength of 1550 nm. The uncertainty in the radius of curvature and subsequently the focal length is ±0.3 mm. Plots of the calculated $c_{2,1}$ coefficients and the focal lengths are shown in Figures 8 and 9. The average focal length (f_{avg}) for these two samples of silicon lenslets is within 4.0% and 3.2% of the design focal lengths for the 16.5mm and 25.7mm lenslets respectively. This difference between the average measured and design focal lengths is due to errors in fabrication etching process. Since the sag of the individual lenslets determines the focal lengths, over or under etching of the lenslets will lead to differences in the focal lengths from the design values. The relative standard deviation (σ_f/f_{avg}) is 1.9% and 3.2% for the 16.5mm and the 25.7mm lenslets respectively. We believe that these variations are due to a combination of measurement and fabrication errors.

4. SUMMARY

We have measured and reconstructed the phase wavefronts in transmission through a selection of our standard fused silica lenslet arrays and in reflection from our silicon lenslet arrays. It is important to note that the Seidel aberrations such as astigmatism, coma and spherical aberration are negligible in both the transmitted and reflected wavefronts from the test lenslet arrays. Furthermore, the average total P-V OPD for the transmitted wavefront through the fused silica lenslets is less than λ/4 and the average RMS wavefront error is less than λ/20. In addition, we have calculated the focal lengths of the silicon lenslets from the reflected wavefront measurements. These calculated values of the focal lengths are well within the design specifications and the variation across the sample population is also within the tolerance for use of these lenslet arrays in a Shack-Hartmann wavefront sensor.

In the future we plan to do a systematic study of the wavefront aberrations in other types of microlenses using the CLAS-2D system. In addition, we plan to make focal length measurements of the fused silica microlenses using both the transmission and reflection setups.

The authors gratefully acknowledge Daniel M. Topa at WaveFront Sciences, Inc. for useful discussions.

REFERENCES

1. L. Erdmann et al, Testing of refractive silicon microlenses by use of a lateral shearing interferometer in transmission," Applied Optics, Vol. 37, No. 4, pp 676-682, 1998
2. D. Malacara, *Optical Shop Testing*, John Wiley&Sons Inc., New York, 1992
3. W.H. Southwell, "Wavefront estimation from Wavefront slope measurements," JOSA **70**(8), 1980